ELSEVIER

Combustion and Flame 133 (2003) 299–310

Combustion and Flame

Suppression limits of low strain rate non-premixed methane flames

M. Bundy[a], A. Hamins[a,*], Ki Yong Lee[b]

[a]*National Institute of Standards and Technology, Gaithersburg, MD 20899-8663*
[b]*School of Mechanical Engineering, Andong National University Andong 770-749, South Korea*

Received 13 August 2002; received in revised form 20 December 2002; accepted 7 January 2003

Abstract

The suppression of low strain rate non-premixed flames was investigated experimentally in a counterflow configuration for laminar flames with minimal conductive heat losses. This was accomplished by varying the velocity ratio of fuel to oxidizer to adjust the flame position such that conductive losses to the burner were reduced and was confirmed by temperature measurements using thermocouples near the reactant ducts. Thin filament pyrometry was used to measure the flame temperature field for a curved diluted methane-air flame near extinction at a global strain rate of 20 s^{-1}. The maximum flame temperature did not change as a function of position along the curved flame surface, suggesting that the local agent concentration required for suppression will not differ significantly along the flame sheet. The concentration of N_2, CO_2, and CF_3Br added to the fuel and the oxidizer streams required to obtain extinction was measured as a function of the global strain rate. In agreement with previous measurements performed under microgravity conditions, limiting non-premixed flame extinction behavior in which the agent concentration obtained a value that insures suppression for all global strain rates was observed. A series of extinction measurements varying the air:fuel velocity ratio showed that the critical N_2 concentration was invariant with this ratio, unless conductive losses were present. In terms of fire safety, the measurements demonstrate the existence of a fundamental limit for suppressant requirements in normal gravity flames, analogous to agent flammability limits in premixed flames. The critical agent volume fraction in the methane fuel stream assuring suppression for all global strain rates was measured to be 0.841 ± 0.01 for N_2, 0.773 ± 0.009 for CO_2, and 0.437 ± 0.005 for CF_3Br. The critical agent volume fraction in the oxidizer stream assuring suppression for all global strain rates was measured as 0.299 ± 0.004 for N_2, 0.187 ± 0.002 for CO_2, and 0.043 ± 0.001 for CF_3Br. © 2003 The Combustion Institute. All rights reserved.

Keywords: Counterflow flames; Extinction; Diffusion flames; Suppression; Temperature measurement; Thin filament; Halon; Low strain rate

1. Introduction

The agent concentration required to achieve the suppression of low strain rate non-premixed flames is an important consideration for fire protection applications as engineers rely on suppression data to estimate suppressant mass requirements for total flooding applications. Information regarding critical suppressant concentrations in the high strain rate regime is less important than in the low strain rate regime, because low strain rate conditions typically require higher agent concentrations and fire protection design must be based on worst-case conditions.

* Corresponding author. Tel.: +1-301-975-6598; fax: +1-301-975-4052.
E-mail address: Anthony.Hamins@nist.gov (A. Hamins).

0010-2180/03/$ – see front matter © 2003 The Combustion Institute. All rights reserved.
doi:10.1016/S0010-2180(03)00012-9

Currently, there is a scarcity of experimental data on the effectiveness of suppressants in low strain rate ($<40\ s^{-1}$) non-premixed flames.

Low strain rate agent suppression requirements in counterflow flames are also of interest because they correspond to agent suppression requirements in buoyancy dominated flames, such as cup burner flames [1]. The burner of choice for testing agent suppression effectiveness has traditionally been the cup burner. In that burner, the flame strain rate is not controlled and preheating of the fuel cup can lead to flame stabilization. A study comparing inert and halocarbon suppressant effectiveness in the counterflow and cup burner geometries was performed by Saso et al. [2]. Their results confirmed the results of Hamins et al. [1], showing a correspondence in flame extinguishment concentration between the cup burner and the counterflow burner at a strain rate of 30 1/s.

The counterflow geometry, is a convenient configuration for direct control of the strain rate and flame position [3]. The effect of flame position on suppressant requirements has been considered in a number of counterflow flame suppression studies. In some counterflow studies, the fuel and oxidizer reactant streams were adjusted such that the flame position is maintained [4]. Flame position was shown to effect suppressant requirements if the flame is too close to the reactant ducts, which was attributed to changes in the velocity profile at the duct exit. Others have investigated suppression of low strain flames. The effectiveness of chemically acting inhibitors on methane-air counterflow diffusion flames was investigated by Vora et al. [5] and Siow et al. [6]. In each of these studies the suppressant effectiveness was related to the measured OH concentration in flames with a global strain rate of $20\ s^{-1}$.

The first comprehensive extinction measurements of very low strain non-premixed flames were reported by Maruta et al. [7], who performed the experiments under micro-gravity conditions. In that study, the extinction of methane-air flames with N_2 added to the fuel stream was investigated using the JAMIC 10 s drop tower. The fuel stream nitrogen concentration required to achieve extinction was measured to increase as the strain rate decreased, until a critical value was obtained. As the global strain rate was further reduced, the required N_2 concentration decreased. This behavior was denoted as a "turning point" and was attributed to the enhanced importance of radiative losses at low strain rates. Numerical calculations were performed to quantify the radiative heat loss effects. The fraction of radiative heat loss to total flame enthalpy was found to be greater than 10% for near extinction flames with a global strain rate less than $4\ s^{-1}$. Several other works to date have established the importance of radiative heat loss on the stability of weakly strained diffusion flames [8-10].

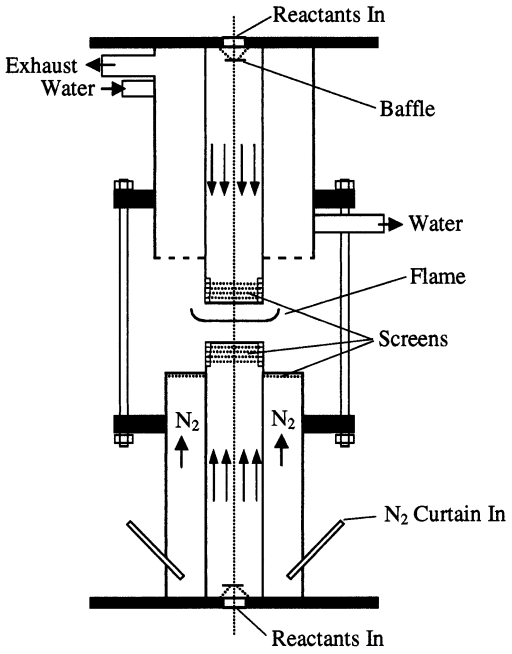

Fig. 1. Schematic drawing of counterflow burner.

The studies that have considered suppression by an agent in normal gravity counterflow flames have not carefully investigated the low strain rate region (see Ref [1] for example). There are experimental difficulties associated with establishing steady flames at low strain rates in the laboratory including flame instabilities associated with ambient currents and forced exhaust. The objective of this study was to study the suppression of low strain rate non-premixed flames in normal gravity through the establishment of steady flames free from significant conductive losses to the burner ducts. In the experiments described here, gaseous N_2 was used as a suppressant to investigate whether turning point behavior occurs in suppression of normal gravity flames, as previously observed in microgravity [7]. In addition, the suppression effectiveness of CO_2 and CF_3Br are also reported for flames with agent added to both the oxidizer and the fuel streams of methane-air diffusion flames.

2. Experimental consideration

Experiments were conducted using the counterflow burner shown in Fig. 1. The inner diameter of the reactant ducts was (23.4 ± 0.1) mm and the duct separation distance was set to (25.0 ± 0.1) mm. Four

200 mesh stainless steel screens were positioned (1.6 ± 0.1) mm from the duct exits and at 1.6 mm intervals to impose a top-hat velocity profile. A water-cooled jacket about the top reactant duct prevented heating of the metal burner and preheating of the reactants. The reactants were air and research grade methane (99.99% purity), which were stored in pressurized cylinders. The oxygen content in the bottled air was measured to be (20.93 ± 0.04)% using a paramagnetic analyzer [11]. The reactant flows were controlled using mass flow controllers that were calibrated using a dry cell primary flow meter with an uncertainty of 1%. The central axis of the burner was aligned vertically with gravity.

The burner was fitted with a concentric tube (64 mm o.d.) about the bottom duct for flow of an inert gas to shield the reactants from ambient air. Experiments were performed using the "curtain" flow of nitrogen to isolate the reactants from the ambient environment. The average velocity of the curtain was tuned to approximately match the fuel flow from the lower duct; however, the magnitude of the curtain flow rate had a negligible effect on the extinction results for curtain flows in the range of 20 cm^3/s to 80 cm^3/s. A number of previous studies investigating the structure and extinction of gaseous diffusion flames applied a flow of nitrogen [12,13] about one of the reactant streams (i.e., a "curtain" of nitrogen), while applying suction through an exhaust section about the opposing reactant stream. Use of a forced exhaust was found to create turbulence in low strain rate flames. Instead, the burner was isolated from ambient disturbances by placing it in a nearly closed compartment (0.5 m × 0.5 m × 0.6 m) with a round 10 cm diameter exhaust port at its top. The compartment was placed inside a chemical hood, allowing controlled removal of combustion byproducts through buoyancy-driven ventilation. The annular top exhaust section of the burner was not used for these experiments.

In the experiments described here, the global strain rate (a_g) was varied from 12 s^{-1} to 120 s^{-1}. The global strain rate concept allows quantification of a characteristic flame residence time or flow time. Suppression measurements were performed by incrementally increasing the agent flow, while maintaining a constant global strain rate. This was accomplished by simultaneously reducing the air or fuel flow. The global strain rate is defined as:

$$a_g = \frac{2V_o}{L}\left(1 + \frac{V_f\sqrt{\rho_f}}{V_o\sqrt{\rho_o}}\right) = \frac{2V_r \cdot V_f}{L}\left(1 + \frac{\sqrt{\rho_f}}{V_r\sqrt{\rho_o}}\right), \quad (1)$$

which is a factor of two larger than the definition used by Maruta et al. [7] or Puri and Seshadri [12]. The parameters V and ρ denote the velocity and density of the reactant streams at the duct boundaries, L is the duct separation distance, and the subscripts O and F represent the oxidizer and fuel streams, respectively. The parameter V_r is defined as equal to V_O/V_F. The expression given by Eq. (1) was derived by Seshadri and Williams [14] to describe the global strain rate for counterflow flames. Seshadri and Williams [14] considered the flames studied by Pandya and Srivastava [15] established at a global strain rate of 20 s^{-1} and found "good agreement" between their theoretical calculations and Pandya's velocity profile measurements. Chelliah et al. [16] used Eq. (1) to compare global and local oxidizer strain rates for undiluted methane-air flames near extinction. Pogliani et al. [17] performed a numerical investigation of flame stretch and radiation on flame extinction at low strain rates. Their results show that there is a proportional relationship between the global and oxidizer side strain rates. Zegers et al. [18] used LDV measurements to determine local strain rates in nonpremixed methane/air and propane/air flames. Their results also show a linear relationship between the maximum velocity gradient on the oxidizer side of the flame and the global strain rate defined by Eq. 1.

The flame extinction measurements conducted here were repeated at least four times. The mean value of the relative expanded standard uncertainty in the agent extinction concentration was typically 2.4% based on repeat measurements and a propagation of uncertainty analysis. All uncertainties reported here are for a coverage factor of two, which is two times the combined standard uncertainty [19]. Measurement repeatability typically accounted for approximately one quarter of the uncertainty.

Changing the velocity of the reactant streams led to changes in flame position and flame shape. Flame shape was characterized in terms of flame curvature through the use of digital photography and image analysis. The curvature was defined as the reciprocal of the average radius of a circle associated with the luminous flame in the cylindrical zone between the ducts. The analysis of curvature was based on three points defined by the intersection of the lower edge of the luminous flame with [1] the central axis and [2] the segments connecting the inner walls of the top and bottom burner ducts.

Temperature measurements were conducted along the centerline near the burner ducts using thermocouples. Heat transfer from the flame to the burner is indicated by the temperature gradient near the burner ducts. The temperature measurements were conducted using small thermocouples with the wires aligned horizontally along an isotherm to minimize conductive losses. Measurements were made using

0.050 mm (0.002 in) diameter (Pt/Pt + 10% Rh) S-type thermocouples. The apparent temperatures were near ambient and a radiative net heat gain was estimated to account for a temperature increase of less than 5 K.

Temperature measurements were performed near the maximum flame temperature using a thin filament pyrometry (TFP) technique. This technique was originally developed by Vilimpoc et al. [20] and is detailed in several publications on laminar diffusion flames [21,22]. A (12.5 ± 2) micron SiC filament was aligned axially between the burner ducts at various radial locations. The radiative energy emitted from the filament was digitally recorded using a CCD camera and close-up lens. The spatial resolution of the image was 0.047 mm/pixel. The image luminous intensity was digitized to 8 bit resolution. The exposure setting on the camera was adjusted so that the image was not saturated (over-exposed) at the maximum flame temperature. Image processing software was used to acquire the fiber intensity data from the digital image. The emission intensity at each axial location was found by subtracting the background intensity from all pixels and integrating the radial intensities across the fiber.

A calibration source was required to determine temperatures from the SiC fiber intensity data. Temperature information was calculated using the OPPDIF computer model at a global strain rate of 68 s^{-1} and nitrogen concentrations of 0.76, 0.78, and 0.80, similar to the method of Ravikrishna et al. [21]. The OPPDIF code uses multi-step chemistry and a narrowband radiation model and has been validated for predicting temperatures in counterflow flames. The radiation model is described in detail by Pogliani et al. [17]. The overall signal measured by the detector, S(T), is a function of the spectral emissive power of the fiber, $E_b(\lambda,T)$, and the wavelength dependent response function of the CCD diode, $R(\lambda)$. A fifth order polynomial least squares fit was found to give the best correlation between the measured signal intensity and the calculated temperature. This is consistent with the correlations reported in the previously noted studies [20-22]. The range of this measurement system was 1450–1800 K with a mean standard uncertainty of 20K based on repeat measurements at the maximum flame temperature.

3. Results and discussion

3.1. Observations

The flames were laminar, steady and the suppression measurements were highly repeatable down to strain rates as low as 12 s^{-1} depending on the agent type and configuration. Below that value, the flames were destabilized due to buoyancy effects. Suppression measurements were made only for steady flames. Undiluted, low strain rate counterflow methane-air flames are yellowish in color. As N_2 and CO_2 were added to either the fuel or oxidizer streams, flame luminosity decreased until near extinction, flame emission was entirely blue in color. This was not the case when CF_3Br was added to the flames. In that case, the flames became increasingly luminous as more agent was added. These flames were yellow and highly luminous near extinction and large amount of soot were observed to escape from the flame.

Figure 2 shows the measured position of the central axis of the luminous flame zone as a function of the global strain rate for several values of the velocity ratio (V_r) when the air stream was flowing from the top duct. In these experiments, the fuel stream was composed of 80% N_2 and 20% CH_4 (by volume), which represents near-extinction conditions. Measurements showed that the measured position of the luminous flame zone changed negligibly as the N_2 concentration was increased from 80% to the percentage necessary to achieve flame extinction. The results in Fig. 1 show that the flames were lifted toward the top duct as the global strain rate was decreased due to the effects of buoyancy. The flame curvature exhibited a maximum as the global strain rate was decreased, whereas the flame position monotonically rose toward the top duct. For example, the $V_r = 3$ flame at $a_g = 20$ s^{-1} exhibited approximately the same flame curvature and location as the $V_r = 1$ flame at $a_g = 40$ s^{-1}.

The results also showed that as V_r was increased from 1 to 4, the luminous flame shifted away from the top duct and the flame curvature generally decreased. Similar trends were observed when the flow orientation was reversed and the air stream flowed from the bottom duct. In that case, it is possible to control flame position by increasing the velocity of the fuel stream relative to the air stream, effectively pushing the flame away from the top fuel duct. This leads, however, to a significant amount of excess fuel that interacts with ambient air, causing afterburning that can preheat the burner and enhance flame stability. For this reason, all suppression measurements reported here are for flames with the oxidizer stream flowing from the top duct. Through adjustment of the value of V_r, the suppression measurements reported here are for flames that were free of significant conductive heat losses.

3.2. Effect of curtain flow on suppression measurements

A number of experiments were conducted to consider the impact of the composition of the ambient

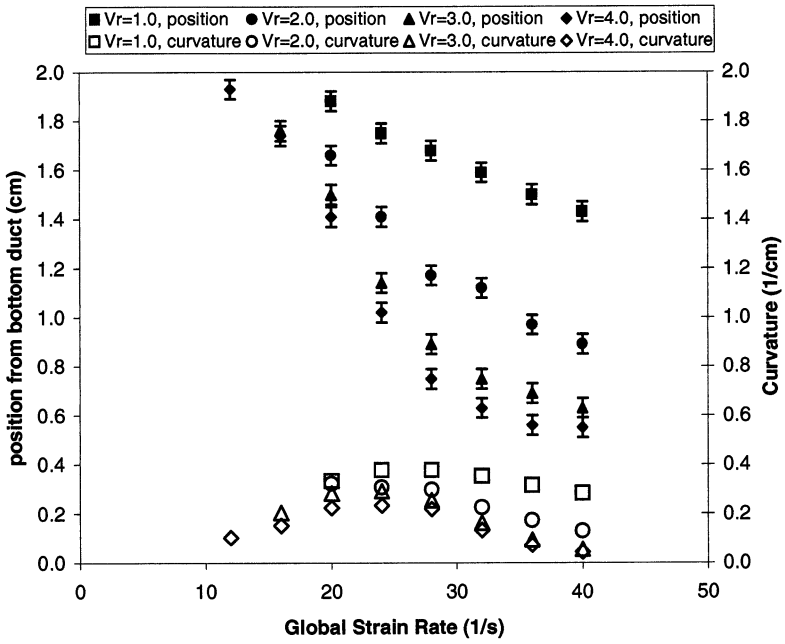

Fig. 2. The position of the luminous flame zone and the flame curvature as a function of the global strain rate for various ratios of the velocity of the air stream to the velocity of the fuel stream (V_r).

environment on flame stability as exemplified by the concentration of suppressant required to achieve extinction. Some studies have used an air ambient [7], whereas others have used an inert environment [13]. Figure 3 shows the critical N_2 volume fraction in the fuel stream required to achieve extinction as a function of the composition of the N_2 curtain for a fixed global strain rate of 20 s^{-1}. As the curtain composition was varied from pure N_2 to pure air, the N_2 concentration in the fuel stream required to achieve

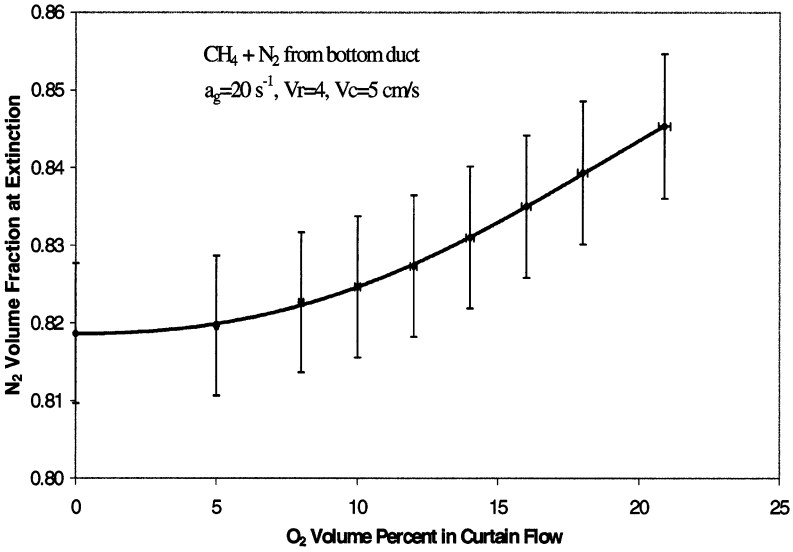

Fig. 3. The measured N_2 volume fraction in the fuel stream required for suppression as a function of the oxygen volume percent in the curtain flow for flames at $a_g = 20\ s^{-1}$ and $V_r = 4$.

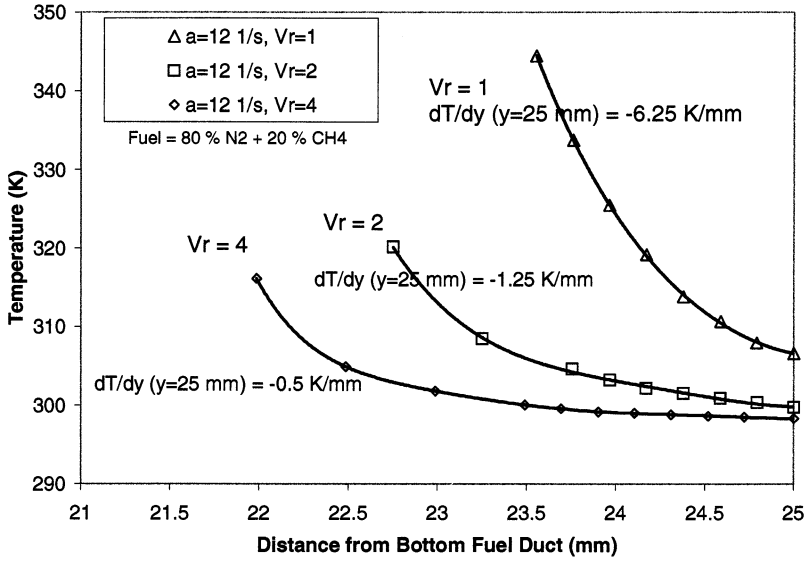

Fig. 4. The measured temperature as a function of location near the air (upper) duct for three near-extinction methane-air flames with N_2 added to the fuel stream under conditions of a constant global strain rate for various values of the air:fuel velocity ratio, V_r.

extinction increased significantly. This suggests that the enhanced stability associated with the air curtain was due to excess fuel reacting with the oxygen in the curtain flow. The ambient composition had a similar effect on the air stream extinction results at a strain rate of 20 s^{-1}, therefore all measurements were performed using a pure N_2 curtain.

3.3. Conductive heat losses to the burner

Thermocouple measurements were conducted to characterize the temperature field near the top reactant duct as V_r was varied. The most problematic conditions in terms of conductive losses are the lowest strain rate flames, which have the broadest tem-

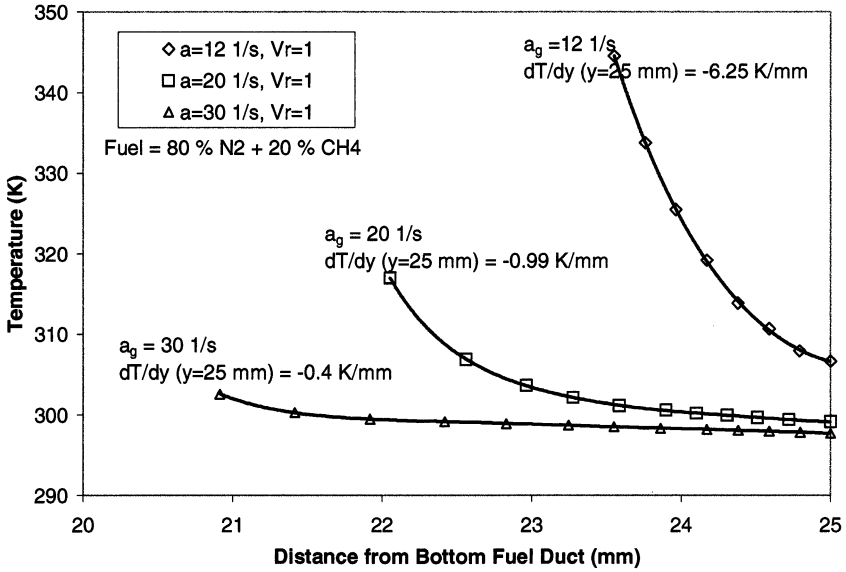

Fig. 5. The measured temperature as a function of location near the air (upper) duct for three near-extinction methane-air flames with N_2 added to the fuel stream under conditions of a constant velocity ratio for various values of the global strain rate.

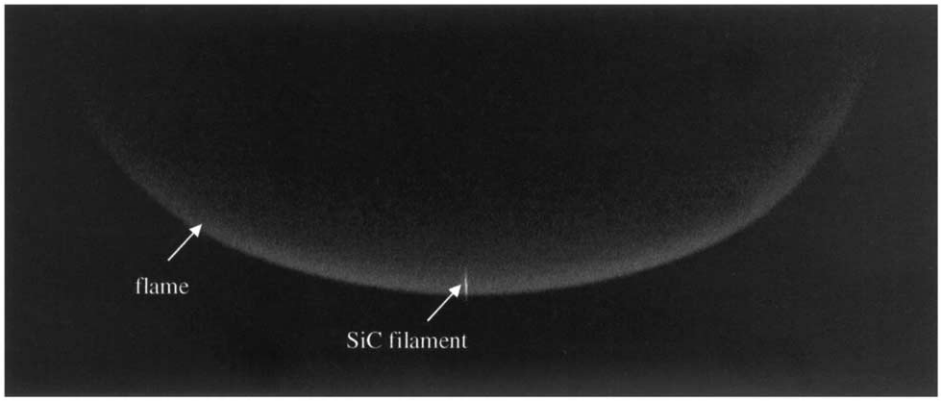

Fig. 6. Superimposed digital images of the flame ant the 12.5 micron SiC filament. The global strain rate, a_g = 20 1/s, and the fuel = 20% CH_4 + 80% N_2, and V_r = 2.

perature profiles and are located closest to the top duct as seen in Fig. 1. Conductive heat losses can be evaluated through consideration of the temperature gradient near the reactant ducts. Figures 4 and 5 show the measured temperature as a function of location near the air (upper) duct for near-extinction methane-air flames with N_2 added to the fuel stream. Figure 4 shows the axial temperature for a constant value of the global strain rate ($a_g = 12\ s^{-1}$) and V_r = 1, 2, and 4. The temperature gradient is negligible for V_r = 4, whereas it is significant for V_r = 1. Figure 5 shows the axial temperature for a constant value of the velocity ratio (V_r = 1) and $a_g = 12\ s^{-1}$, 20 s^{-1}, and 30 s^{-1}. In Fig. 4, the temperature gradient is $<$1 K/mm for $a_g > 30\ s^{-1}$, whereas the gradient is $\gg$1 K/mm for $a_g = 12\ s^{-1}$. There is no single specific value of the temperature gradient that can be considered significant for all flames, since the fractional enthalpy loss from the flame to the burner due to conduction depends on the total flame heat release rate, which varies with flame conditions. In the context of flame suppression, we consider conductive heat loss as significant when the difference in the critical suppressant concentration required to achieve flame extinction is larger than the experimental uncertainty in that quantity.

3.4. Flame temperature measurements

Flame temperatures were attained using luminous emission from a 12.5 micron SiC filament place axially between the burner ducts. A low strain rate flame near extinction (a_g = 20 1/s and C_a = 0.80) was established to observe the effects of curvature and air-fuel velocity ratio on flame structure.

Figure 6 shows the visible blue flame and orange emission from the SiC filament positioned axially along the burner centerline. Two images were superimposed in this figure because the blue flame is not visible when the camera exposure is set to image the fiber. The maximum filament intensity is within 0.5 mm of the lower edge of the visible flame.

The temperature profiles at radial distances of 0.5 mm, 4.4 mm and 11 mm from the burner centerline are shown in Fig. 7. Each profile represents the average of three measurements. Although the flame is curved, the flame temperature profile and peak temperature did not significantly vary with radial position within the volume defined by the burner ducts. The peak flame temperature is indicative of flame enthalpy and thereby flame stability or agent suppressions requirements [23]. This suggests that even though the flames are curved by buoyancy, the local agent concentration required for suppression will not differ significantly along the flame sheet. Further evidence that the flame curvature does not significantly affect the stability of these flames is given by the extinction results described below.

The centerline flame temperature profiles for velocity ratios, V_r, of 1, 2, and 3 are shown in Fig. 8. As expected the position of the maximum flame temperature shifted away from the air side of the burner as V_r was increased. The value of the maximum flame temperature did not change as the velocity ratio was increased from 2 to 3, but the temperature at V_r = 1 was approximately 20 K lower presumably due to conductive enthalpy loss that is evident from Fig. 5. The shape of the temperature profiles indicates that the flame structure is not significantly impacted as the velocity ratio is varied over this range.

3.5. Flame extinction measurements

The temperature measurements described above confirmed that it was possible to avoid significant conductive heat losses to the burner and preserve the

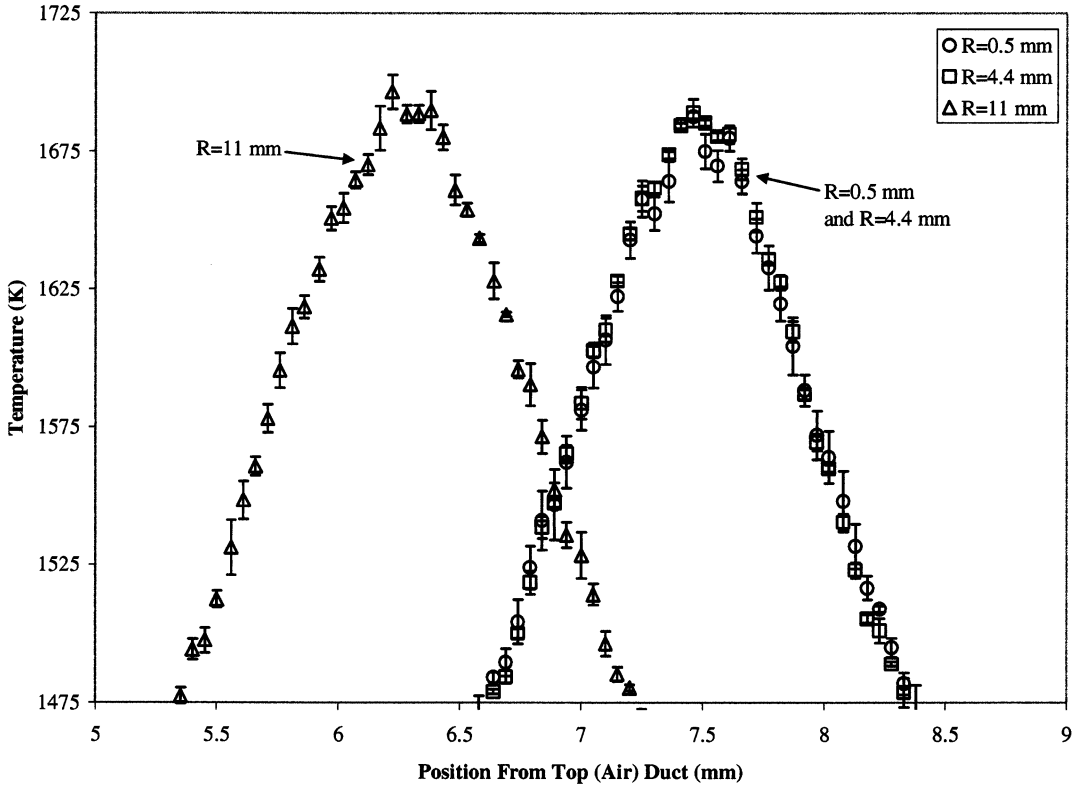

Fig. 7. Three axial temperature profiles from emission of SiC filament at radial locations of the flame that is shown in Fig. 5, a_g = 20 1/s, V_r = 2, C_a = 0.80, The burner diameter is 23.4 mm and the duct separation length is 25 mm.

basic flame structure through control of the ratio of the velocity of the reactant streams (V_r). In this sense, V_r was treated as an independent experimental variable. This notion is explored further in the extinction measurements discussed here, in which the value of V_r was varied from 1 to 4.

Figure 9 shows the measured N_2 volume fraction in the fuel stream required for extinction as a function of the global strain rate for a number of values of V_r for flames without significant conductive heat losses. Conditions below the data points represent stable flames, whereas conditions on and above the data represent flames that have been extinguished. Error bars representing the expanded combined standard uncertainty are shown for all points. Turning point behavior was exhibited, in which the critical suppressant concentration increased as the strain rate decreased, until the concentrations reached a maximum value near a_g = 30 s^{-1} and then decreased as the global strain rate further decreased. For a particular value of the global strain rate, the agent suppression concentration did not significantly change as the velocity ratio was varied. This is consistent with the numerical results of Pogliani et al. [17]. Figure 9 also shows a series of extinction measurements using a duct separation distance of 15 mm, which are in good agreement with the results for L = 25 mm. The L = 15 mm results substantiate the scaling of a_g as a function of V_r and L in Eq. 1.

Flame curvature can affect flame stability, although in counterflow diffusion flames the radius of curvature must be extremely small before there is a noticeable effect. Finke and Grunefeld [24] found measurable differences in the extinction strain rate of hydrogen diffusion flames with a radius of curvature less than 10 mm. The smallest radius of curvature of the flames in this study was 25 mm. Figure 2 shows that the largest absolute difference in flame curvature as V_r was varied from 1 to 4 was observed for a global strain rate of approximately 40 s^{-1}. The measurements in Fig. 8 show negligible differences in N_2 suppression requirements at a_g = 40 s^{-1} as the velocity ratio was varied from V_r = 1 to V_r = 4, suggesting that differences in flame curvature had a negligible effect on agent extinction requirements and flame stability for the flames considered in this study.

Figure 10 shows suppression measurements of the

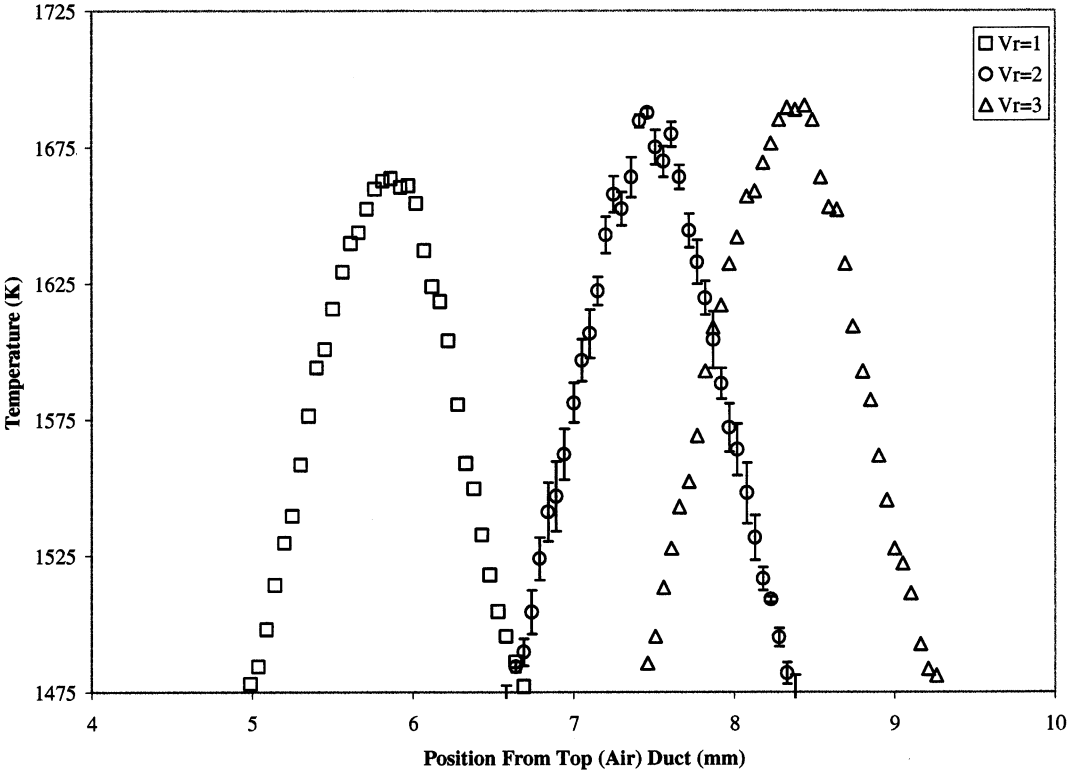

Fig. 8. Centerline temperature profiles from emission of SiC filament at V_r = 1,2 and 3. a_g = 20 1/s, C_a = 0.80.

critical CO_2, and CF_3Br concentration in the fuel stream of nonpremixed CH_4-air flames as a function of the global strain rate. The averaged results for N_2 from Fig. 9 are included in this figure. As expected, the most effective suppressant was CF_3Br, followed by CO_2 and then N_2. The critical suppressant concentration increased as the strain rate decreased, with its value leveling off near 30 s^{-1}, except for CF_3Br, which flattened near 40 s^{-1}. The results demonstrate the existence of turning point behavior for both inert and chemically active agents in normal gravity diffusion flames when agent is added to the fuel stream. The turning point occurs at higher values of a_g than in the microgravity measurements of Maruta et al. [7]. In this regard, buoyancy impacts the structure and relative radiative heat loss of these low strain rate flames.

Figure 11 shows measurements of the N_2, CO_2, and CF_3Br volume fraction in the oxidizer stream required to achieve extinction as a function of the global strain rate. Similar to the results for agent added to the fuel stream (Fig. 9), these measurements also show turning point behavior. Again, the most effective suppressant was CF_3Br, followed by CO_2 and then N_2. The turning point occurs within the same range of global strain rates, at values between 30 s^{-1} to 40 s^{-1}.

Masri et al. [25] suggest that the relevant parameter when comparing agent effectiveness in fuel-stream and air-stream dilution should be the effective mass fraction. The effective mass fraction is defined as the agent mass fraction that would exist at the theoretical stoichiometric flame sheet location in cold flow, neglecting preferential diffusion.

For a methane-air flame, the effective mass fraction is given by: $Y_{eff,st} = Y_{a,f} + (Y_{a,o} - Y_{a,f})\xi_{st}$, where $\xi_{st} = [1 + 4\, Y_{CH4,f}/Y_{O2,o}]^{-1}$. $Y_{eff,st}$ at extinction for both air and fuel-stream dilution is shown in Fig. 12 following the work of Masri [25] and Trees et al. [26]. The fuel-stream dilution extinction experiments from Fig. 10 are represented by the closed symbols in Fig. 12 and the air-stream dilution extinction experiments from Fig. 11 correspond to the open symbols in Fig. 12. For each of the three different agents, air-stream agent addition required a lower amount of agent by mass for extinction than the fuel-stream agent addition. This is consistent with previous measurements by Masri et al. [25] for turbulent non-premixed methane flames in a coflow. Extinction measurements by Trees et al. [26] for laminar non-premixed counterflow methane-air-CF_3Br flames shown in Fig. 12 are also consistent with the results of this study. The differences in

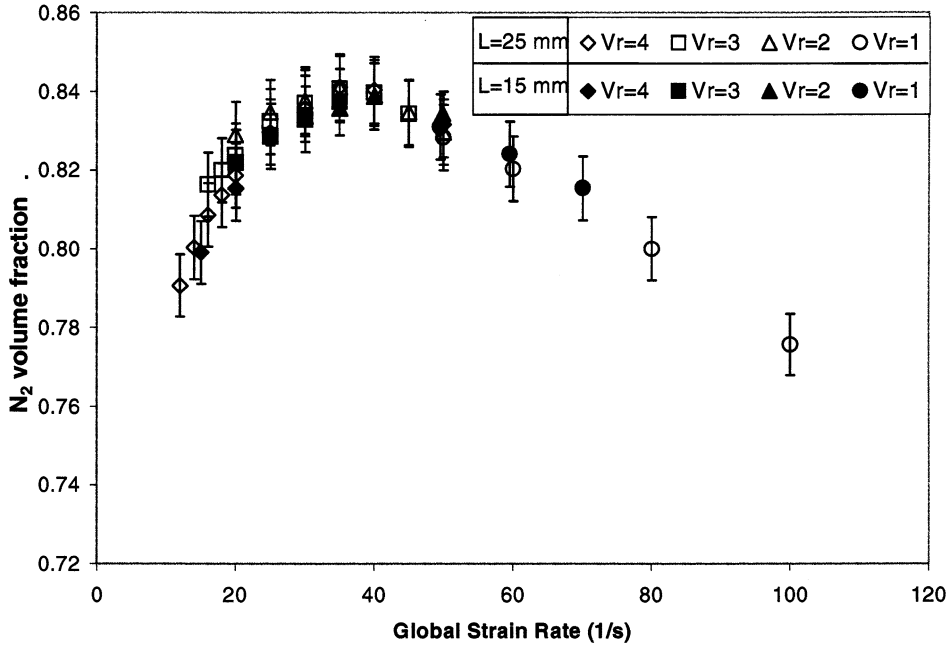

Fig. 9. The measured N_2 volume fraction in the fuel stream required for suppression in flames free of conductive losses as a function of the global strain rate (a_g) for a number of air:fuel velocity ratios (V_r) and two values of the duct separation distance (L) in the presence of a N_2 curtain.

air-stream and fuel-stream agent effectiveness seen in Fig. 12 have been attributed to flame structure and preferential diffusion effects [26].

4. Summary and conclusions

In summary, the range of global strain rates typically investigated in normal gravity was extended by isolating the burner in order to reduce disturbances by ambient currents and by varying the velocity ratio of fuel and oxidizer to reduce conductive losses to the burner. By treating V_r (= V_O/V_F) in Eq. 1 as an independent experimental variable, it is possible to adjust the flame location and thereby minimize conductive heat losses from the flame to the burner. A

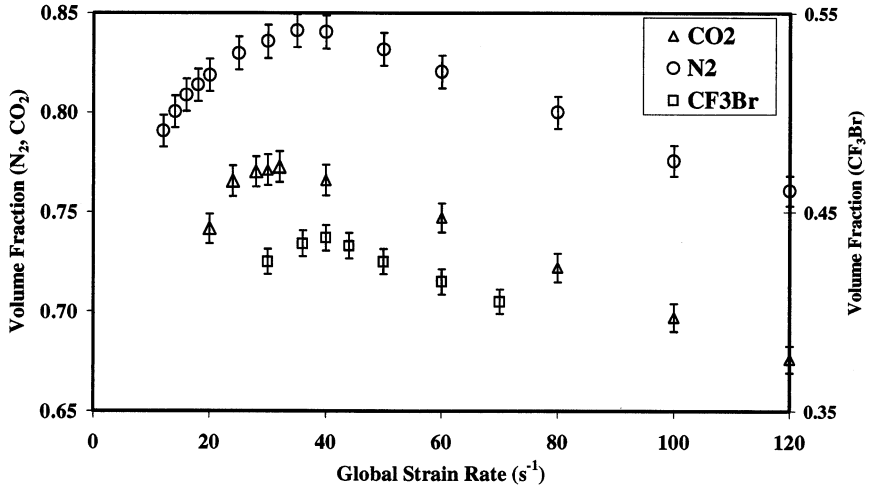

Fig. 10. The critical agent concentration in the fuel stream required for suppression of methane-air diffusion flames as a function of the global strain rate.

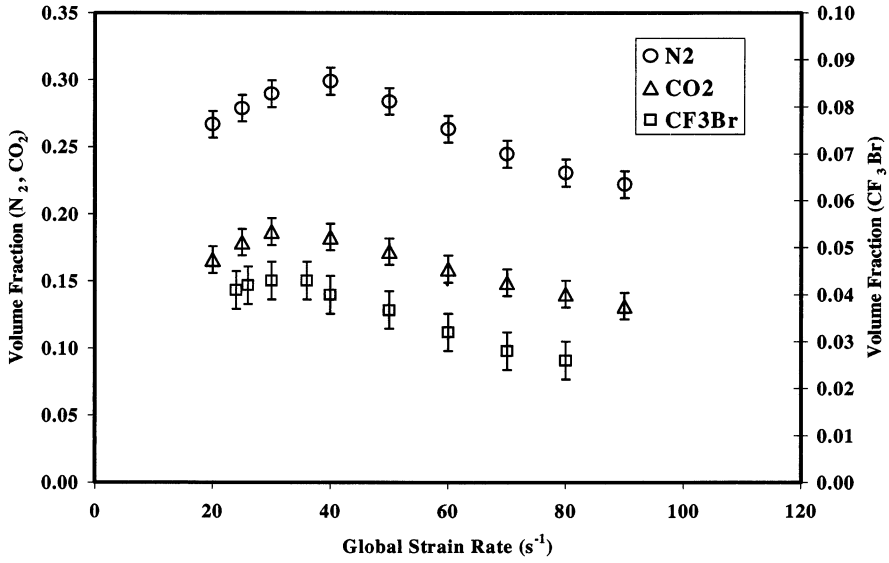

Fig. 11. The critical agent concentration in the oxidizer stream required for suppression of methane-air diffusion flames as a function of the global strain rate.

flame free of conductive losses is relatively more stable than a flame with conductive losses. Such a flame will require larger agent suppression requirements. Whereas flame position and the location of the stagnation point may change as the parameter V_r is varied in these flames, the suppression and maximum flame temperature measurement results suggest that flame stability is essentially unchanged. In addition, the flame temperature measurements show that the maximum temperature does not change locally along the curved flame surface, which suggests that local agent suppressions requirements are invariant along the flame.

The critical concentration of N_2, CO_2, and CF_3Br added to the fuel and oxidizer streams required to obtain extinction of methane-air non-premixed flames was measured as a function of the global strain rate. In terms of fire safety, the measurements demonstrate the existence of a fundamental limit in the suppressant requirements in normal gravity diffusion flames, analogous to agent flammability limits

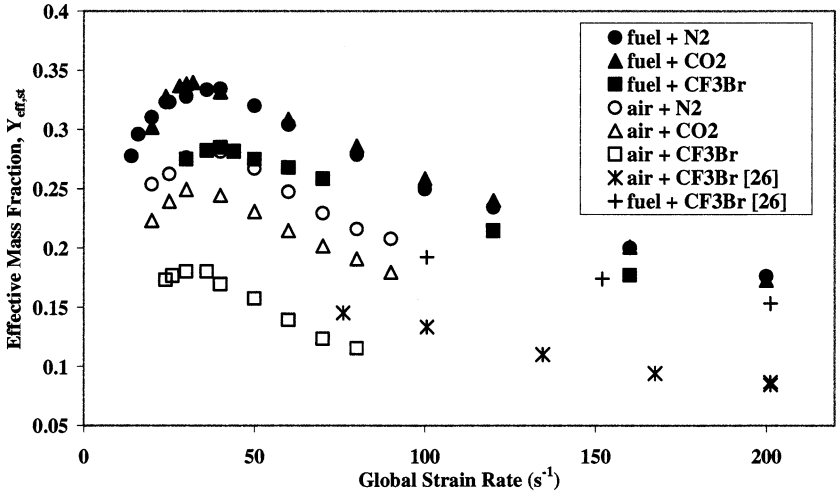

Fig. 12. The critical effective mass fraction required for extinction of methane-air diffusion flames as a function of the global strain rate.

in premixed flames. A fundamental distinction between premixed flammability limits and non-premixed flame suppression limits is that the value of the limiting concentration in a diffusion flame will obtain different values depending on whether the suppressant is added to the oxidizer stream or the fuel stream. The consideration of configuration does not arise in a premixed flame. The critical agent volume fraction in the methane fuel stream assuring suppression for all global strain rates was measured to be 0.841 ± 0.01 for N_2, 0.773 ± 0.009 for CO_2, and 0.437 ± 0.005 for CF_3Br. The critical agent volume fraction in the oxidizer stream assuring suppression for all global strain rates was measured as 0.299 ± 0.004 for N_2, 0.187 ± 0.002 for CO_2, and 0.043 ± 0.001 for CF_3Br.

In terms of suppression by an agent, the peak flame temperature can be thought of as indicative of flame enthalpy and thereby flame stability. Simulations of flame structure using a one-dimensional flame model [27] show that the peak flame temperature is invariant with the reactant velocity ratio for a given global strain rate. Those results are consistent with the suppression and temperature measurements reported here, which show that the agent suppression requirements are invariant with velocity ratio for flames free of conductive losses. The structure of normal and microgravity flames at moderate strain rates can be expected to be similar, as buoyancy effects are relatively unimportant for momentum dominated flames. At low strain rates, however, significant differences in flame structure are anticipated. The ability to work with low strain rate flames in normal gravity enables experimentation at reduced cost as compared to microgravity flames. Further work is ongoing to determine the differences in the structure of low strain rate non-premixed flames under normal and microgravity conditions.

Acknowledgments

We are indebted to William Darko and Mike Kelly of NIST for characterizing the bottled air. The authors are grateful to Professor I.K. Puri of the University of Chicago at Illinois for helpful discussions. This research was partially supported by the NASA Microgravity Research Division through Contract No. C–32,066–T (NIST) with Dr. Sandra L. Olson serving as Technical Monitor. Support for one of the authors (M.B.) through the National Research Council Post-Doctoral Research Associate Program during a portion of this study is acknowledged.

References

[1] A. Hamins, D. Trees, K. Seshadri, H. Chelliah, Combust. Flame 99 (1994) 221.
[2] Y. Saso, N. Saito, L. Chihong, Y. Ogawa, Fire Safety Journal 26 (1996) 303.
[3] H. Tsuji, Prog. Ener. Combust. Sci. 8 (1982) 93–119.
[4] M.A. Macdonald, T.M. Jayaweera, E.M. Fisher, F.C. Gouldin, Combust. Flame 116 (1999) 166–176.
[5] N. Vora, J.E. Siow, N.M. Laurendeau, Combust. Flame 126 (2001) 1393.
[6] J.E. Siow, N.M. Laurendeau, Combust. Sci. Technol. 174 (2002) 91.
[7] K. Maruta, M. Yoshida, H. Guo, Y. Ju, T. Niioka, Combust. Flame 112 (1998) 181.
[8] F. Liu, G.J. Smallwood, Ö.L. Gülder, Y. Ju, Combust. Flame 121 (2000) 275.
[9] J.S. T'ien, Combust. Flame 65 (1986) 31.
[10] S.L. Olsen, J.S. T'ien, Combust. Flame 121 (2000) 439.
[11] M. Kelly, NIST, Report of paramagnetic analyzer test results, personal communication, March 20, 2000.
[12] I.K. Puri, K. Seshadri, Combust. Flame 65 (1986) 137–150.
[13] M.H. Yang, A. Hamins, I.K. Puri, Combust. Flame 98 (1994) 107–122.
[14] K. Seshadri, F.A. Williams, Int. J. Heat Mass Transfer 21 (1978) 251.
[15] T.P. Pandya, N.K. Srivastava, Combust. Sci. Technol. 11 (1975) 165.
[16] H.K. Chelliah, C.K. Law, T. Ueda, M.D. Smooke, F.A. Williams, Twenty-Third Symposium (International) on Combustion The Combustion Institute, Pittsburgh (1990) 503–511.
[17] B. Pogliani, M. Bundy, A. Hamins, I.K. Puri, Proceedings of the Second Joint Meeting of the US Sections of the Combustion Institute, Oakland, 2001.
[18] E.J.P. Zegers, B.A. Williams, E.M. Fisher, J.W. Fleming, R.S. Sheinson, Combust. Flame 121 (2000) 471.
[19] International Organization of Standardization, Guide to the Expression of Uncertainty in Measurement, Geneva, Switzerland, 1993.
[20] V. Vilimpoc, L.P. Goss, B. Sarka, Opt. Lett. 13 (1988) 93–95.
[21] R.V. Ravikrishna, N.M. Laurendeau, Combust. Flame 120 (2000) 372–382.
[22] W.M. Pitts, Twenty-Sixth Symposium (International) on Combustion The Combustion Institute, Pittsburgh (1996) 1171–1179.
[23] R.S. Sheinson, J.E. Penner-Hahn, D. Indritz, The physical and chemical action of fire suppressants, Fire Safety Journal 15 (1989) 43.
[24] H. Finke, G. Grunefeld, Proceedings of the Combustion Institute, Vol. 28 The Combustion Institute, Pittsburgh (2000) 2133.
[25] A.R. Masri, Combust. Sci. Technol. 96 (1994) 189.
[26] D. Trees, A. Grudno, K. Seshadri, Combust. Sci. Technol. 124 (1997) 311.
[27] B. Pogliani, I.K. Puri, A. Hamins, Effect of thermal radiation on the extinction of diluted counterflow nonpremixed flames. Presented at the Western States Section Technical Meeting of the Combustion Institute, Salt Lake City, Utah, October 15-16, 2001.